Structure of Microporous QUI-MnGS-1 and in Situ Studies of Its Formation Using Time-Resolved Synchrotron X-ray Powder Diffraction

Christopher L. Cahill,*,† Younghee Ko,‡ Jonathan C. Hanson,⊥ Kemin Tan,‡ and John B. Parise†,‡

Department of Chemistry, State University of New York, Stony Brook, New York 11794, Department of Geosciences, State University of New York, Stony Brook, New York 11794, and Department of Chemistry, Brookhaven National Laboratory, Upton, New York 11973

Received January 16, 1998

The structure of QUI-MnGS-1 has been determined from single-crystal X-ray diffraction on a ~0.03 × 0.03 × 0.02 mm sample using synchrotron radiation. This material $[(C_7H_{13}N)Mn_{0.25}Ge_{1.75}S_4 \cdot H_2O]$ crystallizes in space group $I\bar{4}2d$ with unit cell $a = 11.581(1)$ and $c = 18.741(3)$ Å. The extended framework of this structure consists of corner-linked $[Ge_4S_{10}]^{4-}$ clusters, the centers of which occupy nodes of a distorted diamond lattice. The 6-rings defined by this lattice form channels that contain the water and organic components of this compound. In situ synchrotron X-ray diffraction studies of its synthesis indicate that an Mn-free precursor phase forms prior to transformation to QUI-MnGS-1. In situ calcination experiments demonstrate that this material is thermally stable to approximately 360 °C.

Materials possessing open framework structures such as aluminosilicate zeolites and other molecular sieves are potentially useful in catalysis, gas separations, molecular recognition, and ion exchange and as solid host lattices.[1,2] Within these structures, TO_4 tetrahedra (T = Al or Si) typically share vertexes to define arrays of channels and pores which are responsible for the unique size and shape selective properties.[1−3] In a departure from this oxide-based chemistry, Bedard introduced a new family of open framework structures based on Ge and Sn sulfide compositions,[4,5] thus inspiring a host of new potential applications.[6−8] With contributions from other research groups, the range of structure types now extends to those consisting of linked M_xS_y clusters such as the $Sb_3S_6^{3-}$ semicube,[9,10] the Sn_3S_4 semicube,[4,5,11−14] the $[Ge_4S_{10}]^{4-}$ adamantine unit,[4,5,15−22] and the $[In_{10}S_{20}]^{10-}$ and $[Sn_{10}S_{20}O_4]^{8-}$ supertetrahedra.[23−25] Several of these materials crystallize with structures resembling the aluminosilicate oxides.[26] The supertetrahedral clusters in the Sn−O−S and In−S systems condense as interwoven cristobalite type nets,[23−25] while analogues of zeolite,[21] neso-,[27] iono-,[28] and tectosilicate[4,5,16,19,21] type structures, are formed in the Ge−S system upon assembly of $[Ge_4S_{10}]^{4-}$ clusters.

Although a complete understanding of the properties and applications of these open framework sulfides

† Department of Chemistry, State University of New York.
‡ Department of Geosciences, State University of New York.
⊥ Brookhaven National Laboratory.

(1) Barrer, R. M. *Hydrothermal Chemistry of Zeolites*; Academic Press: London, 1982.
(2) Breck, D. W. *Zeolite Molecular Sieves*; Krieger: Malabar, FL, 1984.
(3) Ozin, G. A.; Kuperman, A.; Stein, A. *Angew. Chem., Int. Ed. Engl.* **1989**, *28*, 359.
(4) Bedard, R. L.; Wilson, S. T.; Vail, L. D.; Bennett, J. M.; Flanigen, E. M. *The next generation: Synthesis, characterization and structure of metal-sulfide-based microporous solids*; Proceedings of the Zeolites: Facts, Figures, Future. Proceedings of the 8th International Zeolite Conference, Amsterdam, 1989.
(5) Bedard, R. L.; Vail, L. D.; Wilson, S. T.; Flanigen, E. M. U.S. Patent 4,880,761, 1989.
(6) Bedard, R. L.; Vail, L. D.; Wilson, S. T.; Flanigen, E. M. U.S. Patent 4,933,068, 1990.
(7) Ahari, H.; Ozin, G. A.; Bedard, R. L.; Petrov, S.; Young, D. *Adv. Mater.* **1995**, *7*, 370−374.
(8) Ahari, H.; Bowes, C. L.; Jiang, T.; Lough, A.; Ozin, G. A.; Bedard, R. L.; Petrov, S.; Young, D. *Adv. Mater.* **1995**, *7*, 375−378.
(9) Parise, J. B. *Science* **1991**, *251*, 292−294.
(10) Parise, J. B.; Ko, Y. *Chem. Mater.* **1992**, *4*, 1446−1450.
(11) Ko, Y.; Tan, K.; Nellis, D. M.; Koch, S.; Parise, J. B. *J. Solid State Chem.* **1995**, *114*, 506−511.
(12) Jiang, T.; Lough, A. J.; Ozin, G. A.; Young, D. *Chem. Mater.* **1995**, *7*, 245−248.
(13) Jiang, T.; Ozin, G. A.; Bedard, R. L. *Adv. Mater.* **1995**, *7*, 166−70.
(14) Jiang, T.; Ozin, G. A.; Bedard, R. L. *Adv. Mater.* **1994**, *6*, 860−5.
(15) Parise, J. B.; Tan, K. *Chem. Commun.* **1996**, 1687−1688.
(16) Yaghi, O. M.; Sun, Z.; Richardson, D. A.; Groy, T. L. *J. Am. Chem. Soc.* **1994**, *116*, 807−808.
(17) Tan, K.; Ko, Y.; Parise, J. B.; Darovsky, A. *Chem. Mater.* **1996**, *8*, 448−53.
(18) Tan, K.; Darovsky, A.; Parise, J. B. *J. Am. Chem. Soc.* **1995**, *117*, 7039−7040.
(19) Bowes, C. L.; Lough, A. J.; Malek, A.; Ozin, G. A.; Petrov, S.; Young, D. *Chem. Ber.* **1996**, *129*, 283−287.
(20) Bowes, C. L.; Huynh, W. U.; Kirkby, S. J.; Malek, A.; Ozin, G. A.; Petrov, S.; Twardowski, M.; Young, D. *Chem. Mater.* **1996**, *8*, 2147−2152.
(21) Cahill, C. L.; Parise, J. B. *Chem. Mater.* **1997**, *9*, 807−811.
(22) Kirkby, S. J.; Ozin, G. A. *Mater. Res. Soc. Symp. Proc.* **1996**, *431*, 165−170.
(23) Parise, J. B.; Ko., Y. *Chem. Mater.* **1994**, *6*, 718−720.
(24) Parise, J. B.; Ko, Y.; Tan, K.; Nellis, D. M.; Koch, S. *J. Solid State Chem.* **1995**, *117*, 219−228.
(25) Cahill, C. L.; Ko, Y.; Parise, J. B. *Chem. Mater.* In press.
(26) Liebau, F. *Structural Chemistry of Silicates*; Springer-Verlag: Berlin, 1985.
(27) Pivan, J. Y.; Achak, O.; Louer, M.; Louer, D. *Chem. Mater.* **1994**, *6*, 827−830.
(28) Nellis, D. M.; Ko, Y.; Tan, K.; Koch, S.; Parise, J. B. *J. Chem Soc., Chem. Commun.* **1995**, 541−542.

S0897-4756(98)00026-X CCC: $15.00
Published on Web 04/28/1998

requires crystallographic investigations, some such studies have been hampered by the lack of crystals of suitable size for conventional in house diffraction. The title compound, QUI-MnGS-1, is a case in point with only its X-ray powder diffraction pattern reported in the patent literature.[5] Synchrotron X-rays coupled with area detectors have permitted data collection from small crystals of a variety of materials[17,18,29−31] and in the current study has led to the structure determination of QUI-MnGS-1.

Synthetic investigations of framework sulfides often result in mixed phase products. For example, variation in pH with reaction time causes the formation of two different framework types in the DABCO−Mn−Ge−S system,[21] while phase transitions as a function of aging time and uptake of transition metals occurs in the current study of the quinuclidine−Mn−Ge−S system. In situ and time-resolved X-ray diffraction techniques provide insight into the pathways of formation of these materials. Such methods have been previously employed to study a variety of reactions as a function of time and temperature.[32−34] Monitoring the powder diffraction spectra of crystalline species as a reaction progresses yields a time-resolved diffraction pattern, which in turn indicates the order of product (and intermediate) formation as well as provides information regarding the coexistence of phases. We report here the combined use of synchrotron single-crystal and time-resolved in situ X-ray powder diffraction techniques to characterize the reactions occurring in the quinuclidine−Mn−Ge−S system as a function of time and temperature.

Experimental Section

Synthesis. Ex situ syntheses of the QUI-GS-10 **(1)**, QUI-GS-10a **(2)**, and QUI-MnGeS-1 **(3)**[35] compounds were effected in sealed Pyrex tubes at 130 °C under autogenous pressures. A typical reaction mixture for **1** and **2** was 0.2 g of GeS_2 (amorphous), 0.04 g of quinuclidine, and 1.0 g of a 1.0 molar solution of quinuclidine that had been saturated with CO_2(g). Starting mixtures to produce **3** contained, in addition to that for **1** and **2**, 0.02 g of $MnCl_2 \cdot 4H_2O$. Compounds **1** and **2**, both white powders, often cocrystallized within 4−6 h. Longer reaction times resulted in pure samples of **2**. Compound **3**, a yellowish powder crystallized after approximately 18 h as a mixture with **1**. Pure samples of **3** could be obtained after approximately 36 h. All products were washed in ethanol and water and allowed to dry in air at room temperature. Crystals of **2** and **3** suitable for single-crystal diffraction were isolated from single-phase reaction products.

The phases present in each reaction product were identified via X-ray powder diffraction carried out on a Scintag PAD X diffractometer (Cu Kα radiation), and the resulting powder patterns were compared with those reported in the patent literature.[5] Elemental analysis of **3** gave weight percentages: 20.26% carbon, 3.72% hydrogen, 3.34% nitrogen, 34.12% sulfur, 3.88% manganese, and 30.78% germanium. The weight percentage of oxygen could not be determined in the presence of manganese and was therefore estimated to be the remaining 3.9%. A qualitative electron microprobe analysis of **1** and **2** indicated the presence of Ge and S, and no manganese.

Thermogravimetric analysis of a powder of **3** was performed on a Perkin-Elmer 7 Series Thermal Analysis system in flowing nitrogen with a heating rate of 5.0 °C/min over the range 30−600 °C. A single weight loss event of approximately 30% of the total mass of the sample begins at 250 °C and is complete by 425 °C.

Structure Determination

Synchrotron/Imaging Plate Data Collection and Processing. Two separate data sets were collected at beamline X3A1 of the National Synchrotron Light Source (NSLS) on two different crystals of **3**: one at 298 K and another at 18 K. For the room temperature study, a 0.03 × 0.03 × 0.02 mm crystal was mounted on a quartz fiber and a set of 20 reflections in the range $14.5° < 2\theta < 31.6°$ ($\lambda = 0.632$ Å) were measured with a scintillation counter to determine a precise unit cell ($a = 11.677(1)$ and $c = 18.908(3)$ Å) and orientation matrix. The scintillation counter was then replaced with an imaging plate cassette in order to collect intensity data. Data were collected and processed as described previously.[17,29] Examination of the systematic absences in the reflection file indicated the space group was either $I4_1md$ (109) or $I\bar{4}2d$ (122); $I\bar{4}2d$ was chosen and structure solution proceeded via direct methods. Checks for missing symmetry confirmed the space group choice, and subsequent refinements were carried out with SHELXL93.[36]

The low-temperature study of this material was performed in an attempt to learn more about the extraframework organic component of the structure (see discussion section). For this experiment, a second crystal of **3** was mounted on a triad of three ∼10 μm graphite fibers. A Displex cryostat cooled the sample to 18 ± 5 K for imaging plate (IP) data collection. Each imaging plate was indexed and integrated with the program Denzo,[37,38] and a tetragonal unit cell ($a = 11.581(1)$ and $c = 18.741(3)$ Å) was obtained. The reflection intensities from each imaging plate were scaled to one another with Scalepack[38] to account for decay of the synchrotron beam. Examination of the reflection indices indicated a space group consistent with the room temperature study ($I\bar{4}2d$). A summary of experimental conditions and refinement results is given in Table 1. A structural model identical to that from the room temperature study was obtained after direct methods solution (SHELXS86)[39] and refinement with SHELXL93.[36] Several reflections with unreasonable differences between F_c and F_o were attributed to interference from the beamstop and graphite fibers and were omitted from the refinement. Refinement suggested that a racemic twin was present, and such was

(29) Tan, K.; Ko, Y.; Parise, J. B.; Park, J.-H.; Darovsky, A. *Chem. Mater.* **1996**, *8*, 2510−2515.
(30) Neder, R. B.; Burghammer, M.; Grasl, T.; Schulz, H. *Z. Kristallogr.* **1996**, *211*, 591−593.
(31) Neder, R. B.; Burghammer, M.; Grasl, T.; Schulz, H. *Z. Kristallogr.* **1996**, *211*, 763−765.
(32) Francis, R. J.; Price, S. J.; Evans, J. S. O.; O'Brien, S.; O'Hare, D.; Clark, S. M. *Chem. Mater.* **1996**, *8*, 2102−2108.
(33) Grey, C. P.; Poshni, F. I.; Gualtieri, A. F.; Norby, P.; Hanson, J. C.; Corbin, D. R. *J. Am. Chem. Soc.* **1997**.
(34) Gualtieri, A.; Norby, P.; Artioli, G.; Hanson, J. C. *Phys. Chem. Miner.* **1997**, *24*, 191−199.
(35) This system of nomenclature is explained in the patent literature found in ref 5.
(36) Sheldrick, G. M. SHELXL93, Program for the Refinement of Crystal Structures, University of Gottinggen, Germany, 1993.
(37) Minor, W. XDISPLAYF Program, Purdue University, 1993.
(38) Otwinowski, Z. *Oscillation Data Reduction Program*, Proceedings of the CCP4 Study Weekend: Data Collection and Processing, SERC Daersbury Laboratory, England, January 29−30, 1993.
(39) Sheldrick, G. M. SHELXS86, Program for the Solution of Crystal Structures, University of Gottinggen, Germany, 1986.

Table 1. Crystal Data and Structure Refinement for QUI-MnGS-1 (3)

Crystal Data	
empirical formula	$(C_7H_{13}N)Mn_{0.25}Ge_{1.75}S_4.H_2O$
formula weight	398.24
crystal system	tetragonal
space group	$I\bar{4}2d$
unit cell dimensions (Å)	$a = 11.581(1)$, $c = 18.741(3)$
volume of unit cell, Z	2578.2(8) Å^3, 8
density (calculated)	2.10 g cm^{-3}
radiation type and wavelength	Synchrotron, 0.643 Å
measurement temperature	18 ± 5 K
crystal size, shape, color	~0.03 × 0.03 × 0.02 mm, triangular plate, colorless
Data Collection	
data collection method	imaging plate
scanner	Fuji, Bio-imaging analyzer, BAS2000
2θ offset of imaging plate cassette	0°
crystal to imaging plate distance	200 mm
no. images exposed	60
oscillation angle	10°
overlap angle	2°
Phi range	360
gradation and latitude	1024, 4
resolution	100 μm
sensitivity	10000
no. reflns collected ($I > 1.0\sigma I$)	8767
merge R (based on I)	0.0602
max value of (sin θ)/λ	0.63
max/min h,k,l	±13, ±14, ±21
absorption coeff	37.27 cm^{-1}
absorption corr	none
Refinement	
refinement on	F^2
no. reflns used	1037
final R indices ($I > 4\sigma I$)	R1[a] = 0.0576, wR2[b] = 0.1424
R indices (all data)	R1 = 0.0639, wR2 = 0.1569
GOF for all integrated reflns	1.196
no. of params refined	31
residual electron densities (peak and hole)	1.684 and −0.615 (e Å^{-3})

[a] $R1 = \sum||F_o| - |F_c||/\sum|F_o|$. [b] $wR2 = [\sum[w(F_o^2 - F_c^2)^2]/\sum[w(F_o^2)^2]]^{1/2}$.

refined to a 0.17(4) fractional contribution. Since $I\bar{4}2d$ is an acentric space group, the absolute configuration was determined. As in the room temperature study, no ordered guest molecules were located in the extraframework region of this material (see discussion section).

In Situ Powder Diffraction. Experiments to study reaction pathways in the quinuclidine−Mn−Ge−S system were carried out at the X7B beamline at the NSLS. The experimental setup for in situ X-ray powder diffraction experiments has been described in detail previously,[40−42] and a schematic of the apparatus appears in Figure 1. For these experiments, temperature was varied using an air heater while hydrothermal conditions were maintained inside a 0.7 mm quartz capillary using an overpressure of N_2(g). A slurry of the starting mixture for **3** was loaded into the capillary and the temperature ramped to 180 °C over 90 min. The imaging plate was driven laterally at a rate of 0.4 mm/min. The exposed plates were read on a Fuji BAS2000 scanner and the data extracted using Interactive Data Language (IDL) routines generated and maintained by the beamline staff.

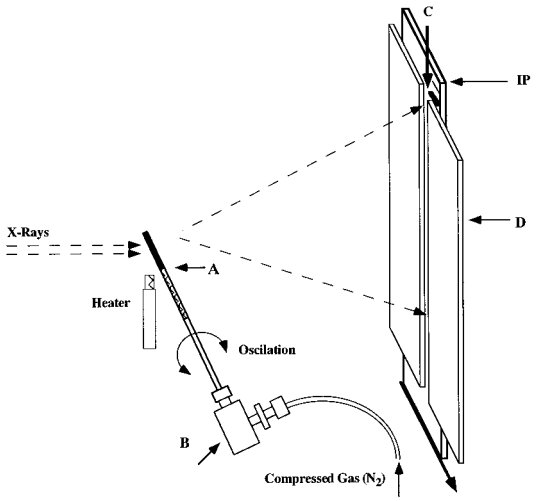

Figure 1. The in situ, time-resolved X-ray powder diffraction apparatus at the X7B beamline of the NSLS. Sample slurries are loaded into a 0.7 mm quartz capillary (A) and heated via an air heater. The capillary is held in place with a Swagelock (B) fitting mounted on a modified goniometer head. Hydrothermal conditions are maintained with an overpressure of N_2 gas. Diffracted X-rays are collected on a portion (C) of the imaging plate (IP) that is defined by two lead shields (D). The IP is translated (bold arrow) to expose fresh portions of the plate and obtain diffraction data as a function of time. Alternatively, a ceramic resistance heater can replace the air heater, and a vacuum line can replace the N_2 overpressure for the high-temperature calcination studies.

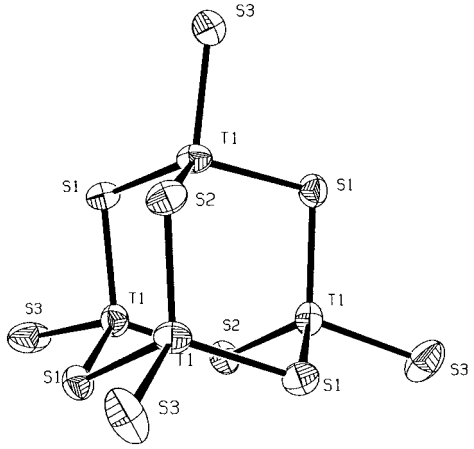

Figure 2. ORTEP[47] representation of the $[Ge_4S_{10}]^{4-}$ found in QUI-(Mn)GS-1 (**3**).

Calcination experiments were carried out in the same apparatus after replacing the N_2 overpressure with a vacuum line, and switching to a high-temperature ceramic heater (Figure 1). A previously synthesized sample of **3** was loaded into a 0.7 mm quartz capillary and ramped from 90 to 500 °C over 6 h under a vacuum of 30 mTorr.

Results and Discussion

The structure (Tables 2−4) of **3** (QUI-MnGS-1) contains 4-connected $[Ge_4S_{10}]^{4-}$ clusters (Figure 2)[47] which corner link to form 6-ring channels that run along [111] (Figure 3). Visualization of this connectivity may best

(40) Norby, P. *Mater. Sci. Forum* **1996**, *228−231*, 147−152.
(41) Norby, P. *J. Appl. Crystallogr.* **1997**, *30*, 21−30.
(42) Parise, J. B.; Tan, K.; Norby, P.; Ko, Y.; Cahill, C. L. *Mater. Res. Soc. Symp. Proc.* **1996**, *453*.
(43) Meier, W. M.; Olson, D. H.; Baerlocher, C. *Atlas of Zeolite Structure Types*; Butterworth: London, 1996.

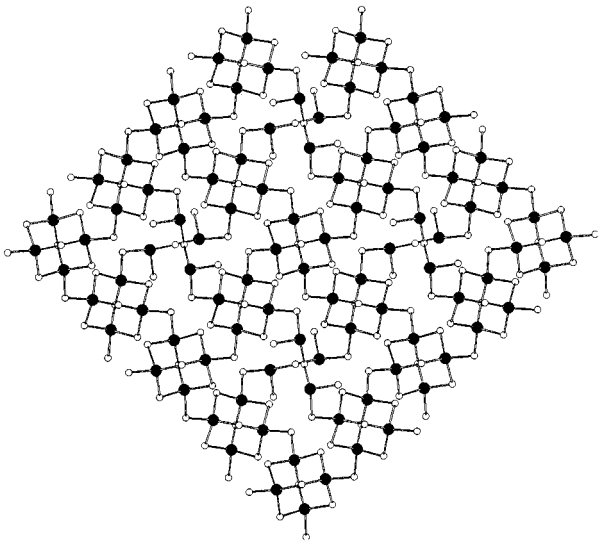

Figure 3. The 3-D extended framework of **3** shown approximately down [116]. Black circles are the T sites, while open circles are S atoms. Each $[Ge_4S_{10}]^{4-}$ cluster is corner linked to four different clusters

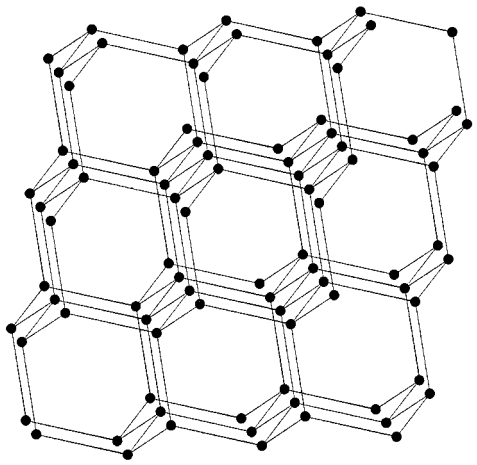

Figure 4. A nodal representation of **3** where each $[Ge_4S_{10}]^{4-}$ cluster has been replaced with a single atom and connecting T−S−T linkages have been replaced with straight lines. This representation exposes a single diamond-type lattice.

be achieved if the center of each cluster is replaced by a single node and the corner linking T−S−T units are replaced by straight lines.[43] Using this simplification, a single diamond lattice emerges (Figure 4); diamond lattices in open frameworks are common.[5,16,19] For example, Yaghi et al. reported a structure in which the nodes of the diamond net are occupied by $[Ge_4S_{10}]^{4-}$ clusters and $[MnS_4]^{4-}$ tetrahedra.[16] For **3** however, there are no tetrahedral transition metal centers to link the clusters. Rather, each cluster is corner linked to another via apical sulfur bridges.

Selected bond lengths and angles appear in Table 3. As seen in other materials containing $[Ge_4S_{10}]^{4-}$ clusters,[16−18,20,21,27] the apical T1−S3 (Figure 2) distances are shorter than the intracluster T−S bonds. For materials in which transition metal centers link $[Ge_4S_{10}]^{4-}$ clusters, this shortening has been attributed to the underbonding of S atoms coordinated to both a metal and to Ge. In the title compound, however, the absence of linking transition metal centers (Figure 3) minimizes this effect and the bridging T−S bond lengths

Table 2. Atomic Coordinates (Å × 10⁴) and Equivalent Isotropic Displacement Parameters (Å² × 10³) for QUI-MnGS-1[a] (3)

atom	*x*	*y*	*z*	*U*(eq)
T[b]	839(1)	3755(1)	1834(1)	32(1)
S(1)	−463(2)	2770(2)	2485(1)	32(1)
S(2)	0	5000	1075(2)	35(1)
S(3)	1955(4)	2500	1250	54(1)

[a] *U*(eq) is defined as one-third of the trace of the orthogonalized U_{ij} tensor. [b] T is the tetrahedrally coordinated metal sites containing $Ge_{0.875}$ and $Mn_{0.125}$.

Table 3. Selected Bond Lengths (Å) and Angles (deg) for QUI-MnGS-1 (3)[a]

T−S(3)	2.232(3)
T−S(2)	2.246(3)
T−S(1)[a]	2.248(3)
T−S(1)	2.250(3)
S(3)−T−S(2)	110.99(9)
S(3)−T−S(1)[a]	97.21(12)
S(2)−T−S(1)[a]	114.27(9)
S(1)−T−S(3)	108.90(9)
S(2)−T−S(1)	112.29(8)
S(1)[a]−T−S(1)	112.12(6)
T[b]−S(1)−T	102.40(11)
T−S(2)−T[c]	101.44(16)
T[d]−S(3)−T	109.16(18)

[a] Symmetry transformations used to generate equivalent atoms: [a] $-y + 1/2, x + 1/2, -z + 1/2$ [b] $y - 1/2, -x + 1/2, -z + 1/2$; [c] $-x, -y + 1, z$; [d] $x, -y + 1/2, -z + 1/4$.

Table 4. Anisotropic Displacement Parameters[a] (Å² × 10³) for QUI-MnGS-1 (3)

	U_{11}	U_{22}	U_{33}	U_{23}	U_{13}	U_{12}
T	35(1)	33(1)	−2(1)	0(1)	7(1)	28(1)
S(1)	37(1)	27(1)	32(1)	−4(1)	2(1)	3(1)
S(2)	46(2)	29(2)	31(2)	0	0	2(2)
S(3)	30(2)	63(3)	67(3)	−26(2)	0	0

[a] $U_{ij} = \exp\{-2\pi^2[h^2a^2U_{11} + ... + 2hkabU_{12}]\}$.

more closely resemble those of the intracluster T−S lengths: 2.232 Å apical T−S vs an average of 2.248 Å for intracluster.

Although most S−T1−S bond angles are close to the ideal expected for tetrahedral geometry, strain associated with the formation of the 6-ring channel (Figure 3) is seen in the (S(3)−T−S(1)[a]) linkage (Table 3). Such strain has been observed in other framework Ge−S compounds, but has usually been present in the S−M−S linkages of the transition metal components. In the absence of these building units, as is the case for **3**, ring strain is manifested in S−T−S bond angles, primarily in S(3)−T−S(1)[a].

The asymmetric unit of **3** contains one tetrahedrally coordinated metal site. The Mn atoms were assumed to be disordered over this site on the basis of a lack of diffraction evidence for ordering. X-rays are unlikely to distinguish between Ge and Mn given their proximity in atomic number (25 and 32, respectively) and the small weight percentage of Mn (3.88%). Germanium and Mn were thus constrained to occupy the same atomic position with a fixed total occupancy for the site of 1.0. Site fractions of each element were estimated from chemical analysis and were 0.125 and 0.875 for Mn and Ge, respectively.

On the basis of the TGA data and elemental analysis, it is estimated that approximately 30 wt % of **3** is organic constituents and H_2O, giving a final empirical

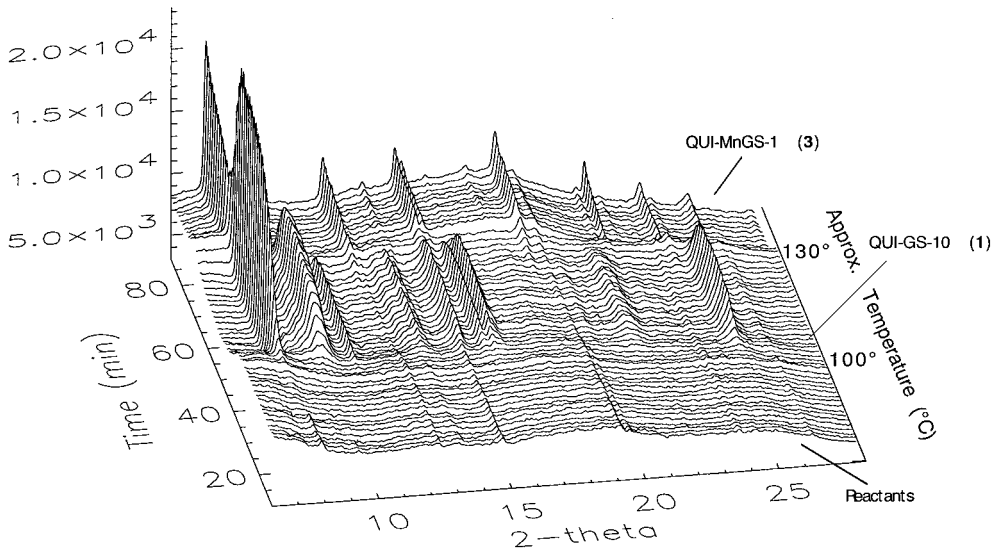

Figure 5. In situ time-resolved X-ray diffraction spectra of the hydrothermal growth of **3**. Time and approximate temperature are shown into the page, while 2θ and arbitrary intensity are shown in the plane of the paper. During a temperature ramp, the appearance of **1** (QUI-GS-10) occurs at approximately 100 °C, while transformation to **3** begins at 130 °C and is complete by 150 °C. This transition is coupled with the uptake of Mn from the reactant slurry.

formula of $(C_7H_{13}N)Mn_{0.25}Ge_{1.75}S_4 \cdot H_2O$. The TGA data do not support a loss of surface water (i.e. no weight loss below 100 °C); therefore it is assumed that the water molecules are tightly bound and are removed from the structure during the same event as the loss of quinuclidine. These molecules were not explicitly located within the structure of **3** in either the room temperature or 18 K X-ray study as it is likely they decomposed during synthesis and the resultant products are disordered over the void space defined by the framework. Decomposition of the organic component of framework sulfide materials has been noted previously.[23,25]

The time-resolved X-ray diffraction (Figure 1) spectra for the in situ synthesis of **3** is shown in Figure 4. During a temperature ramp, diffraction peaks corresponding to **1** appear at approximately 100 °C. This material proceeds through a less crystalline intermediate at approximately 130 °C before a complete transition to **3** at 150 °C. This phase transition is assumed to be coupled with the uptake of Mn ions from the reactant slurry, as EPMA of ex situ prepared samples of **1** and **3** show only **3** to contain manganese. Control experiments without Mn present show the formation of **1** only and no transformation to **3**.

Ex situ syntheses of **3** often result in mixed phase products, yet no coexistence of **1** and **3** is seen in the in situ diffraction pattern, nor is there any evidence of the formation of **2**. This may be due to the nature of the small capillary reaction cell which could inhibit diffusion of reactants into the region sampled. Ex situ methods utilize larger Pyrex tube reaction vessels and allow for a more dynamic reactant slurry and hence a range of compositional gradients. X-ray analysis of end products would include contributions from all crystalline species formed in different regions of the tube. In situ sampling, on the other hand, follows a limited composition over a small (1.0−2.0 mm) area. Further, **2** may form only upon quenching, in which case its formation would be seen only in ex situ preparations.

In situ calcination of **3**, as studied via time-resolved X-ray experiments (Figure 1), indicates that the removal of the organic component of this material begins at approximately 240 °C. The evidence for this is a increase of the (101) peak (Figure 6) as disordered molecules are no longer destructively contributing to the scattering. At approximately 360 °C, the intensity of the (101) begins to decrease rapidly, indicating that the framework is no longer stable at this temperature. The collapse of the framework is complete at approximately 430 °C. These temperatures are consistent with those obtained via TGA.

To further illustrate this behavior, powder diffraction patterns of **3** were calculated[44] with and without an organic component. Although the organic species were not explicitly located in **3** (see above), carbon and oxygen atoms were placed at Fourier peaks in a map of the framework region strictly for calculation purposes. The resulting calculated patterns are shown in Figure 6 (inset). The model containing an organic guest shows a significant decrease in intensity of the (101) reflection with respect to the organic-free model. The observed increase in intensity of this peak during the in situ calcination experiment is thus a result of organic guest removal. Similar peak intensity phenomena are seen during in situ zeolite dehydration and gas desorption experiments.[45,46]

The in situ experiment of the current study (Figure 6) demonstrates that there is a temperature range (240−360 °C) in which a portion of the organic is removed without destruction of the framework. The subsequent collapse of the extended structure of **3** is similar to that observed by Bowes et al.[19] in the structurally related TMA-FeGeS (TMA = tetramethyl-

(44) Larson, A. C.; Dreele, R. B. V. *GSAS: General Structure Analysis System*; Los Alamos, NM 87485, 1986.

(45) Grey, C. P. Personal communication.
(46) Norby, P. Personal communication.
(47) Johnson, C. K. Oak Ridge Thermal Ellipsoid Program, Oak Ridge National Laboratory, Oak Ridge, TN, 1965.

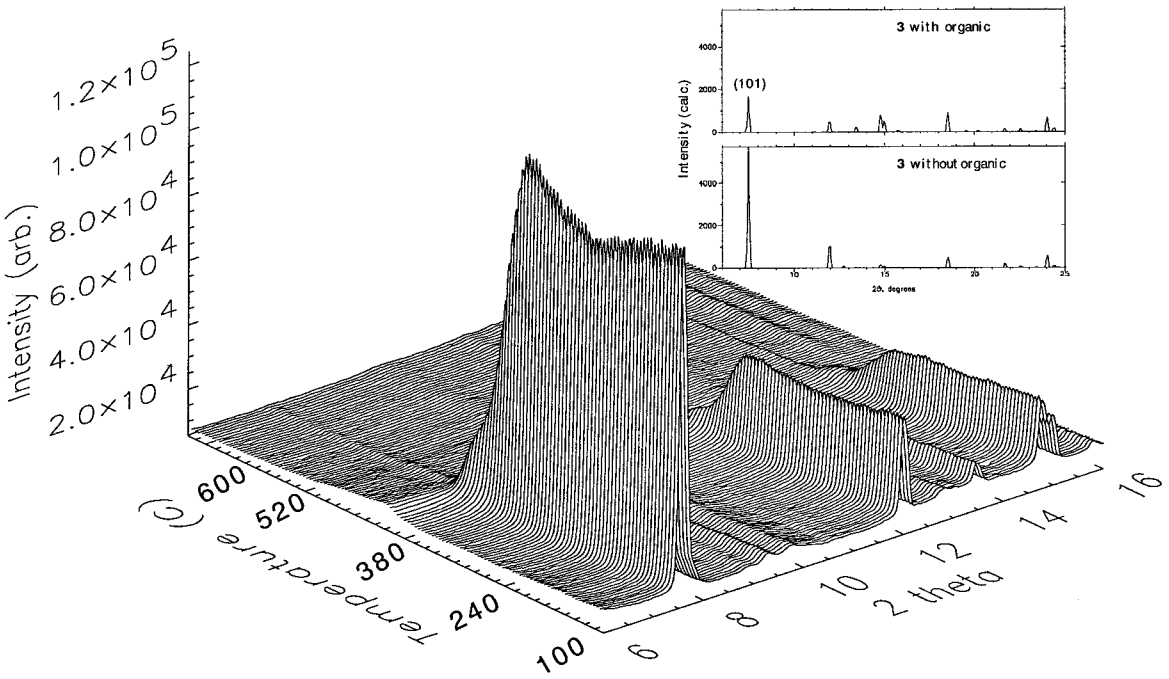

Figure 6. In situ time-resolved X-ray diffraction spectra of the calcination of **3**. An ex situ prepared sample of **3** was ramped from 100 to 600 °C under vacuum over 6 h. The increase in intensity of the (101) reflection ($2\theta = 7.4$) beginning at 240 °C is due the removal of the organic guest species prior to structural collapse at 360 °C. Calculated diffraction patterns with and without organic components (inset; top and bottom respectively) are shown to illustrate this effect.

ammonium) material. They report stability to approximately 400 °C when studied under similar (vacuum) conditions.

A preliminary structure of **2** was determined from data collected on a Siemens Smart platform CCD diffractometer. This material crystallizes as a chain structure analogous to the previously reported DPA-GS-8.[28] The data collected for **2** was of insufficient quality for a thorough refinement, and a synchrotron study is underway to finalize structural differences between this and other chain structure Ge−S materials. Crystals of **1** suitable for structure analysis have not yet been obtained as this material quickly transforms to **2** (QUI-GS-10a) in the absence of Mn or to **3** (QUI-MnGS-1) in preparations containing Mn.

Conclusion

Synchrotron radiation has allowed determination of the structure of QUI-MnGS-1: a material that had remained structurally unknown due to small crystal size. The formation of this material was studied via in situ synchrotron X-ray diffraction, and this demonstrated the formation of an Mn-free precursor phase (QUI-GS-10) prior to transformation to the title compound. The phase transition to QUI-MnGS-1 is observed to be coupled with the uptake of Mn from the reactant mixture. Time-resolved in situ X-ray calcination experiments show that **3** (QUI-MnGS-1) exhibits partial organic removal prior to structural collapse.

Acknowledgment. We thank the NSF (Grant DMR 94-13003) for financial support. Research carried out in part at the National Synchrotron Light Source at Brookhaven National Laboratory is supported by the U.S. Department of Energy, Division of Materials Sciences and Division of Chemical Sciences. The SUNY X3 beamline is supported by the Division of Basic Energy Sciences of the U.S. Department of Energy (DE-FG02-86ER45231), while beamline X7B is supported under contract DE-AC02-76CH00016 with the U.S. Department of Energy, Division of Chemical Sciences. The authors are grateful to Guang Wu for assistance at the beamline and to Poul Norby whose contribution to the development of in situ measurements at X7B helped make these experiments possible.

Supporting Information Available: Structure factors for QUI-MnGS-1 (**3**) (14 pages). See any current masthead page for ordering instructions.

CM980026D